2D NUMERICAL MODELING OF WAVE TRANSFORMATION ON SOFT MUDDY BEDS

Ali Oveisy [1] , Mohsen Soltanpour [2]

1-Formerly, Graduate Student, Civil Eng. Department, K. N. Toosi University of Technology
2-Dr. Eng., Assistant Professor, Civil Eng. Department, K. N. Toosi University of Technology

Abstract

The present paper offers a numerical model which can be applied for the simulation of wave height distribution on a 2-D horizontal soft mud layer. The model is based on mild slope equations and it includes combined wave refraction, diffraction, reflection and breaking. The high energy dissipation of wave height due to the presence of fluid mud layer has also been simulated. Wave height attenuation is calculated from a multi-layered wave-mud interaction model considering the vertical distribution of water content ratio in fluid mud layer. The constitutive equations of visco-elastic-plastic model are assumed for the rheological behavior of fluid mud. An artificial neural network is used as a part of wave attenuation calculation to speed up the computation. Applying the model in the East Bay, Louisiana at the mouth of Mississippi River shows a reasonable agreement with the wave height measurements.

Keywords: Fluid mud, Visco-elastic-plastic model, Wave attenuation, Wave_mud interaction, Artificial neural network

Introduction

It is well known that water surface waves and muddy beds interact to exert influence on each other. While the wave-damping rate is observed by the presence of bottom mud, the mud is transported by the inter-surface wave induced by the surface waves. Both effects are of practical importance, and the problem of interaction between water waves and bottom mud has long been drawing attention.

During the past decades, a number of studies have been conducted on different aspects of wave-mud interaction including two most important phenomena, i.e. wave attenuation and mud mass transport [1-5]. However, almost all of these studies have been conducted on horizontal beds under laboratory conditions. There have also been few efforts to consider the effect of bottom slope on wave transformation and mud mass transport [5]. In order to approach the real field problems, where the changes of cross-shore profiles along the shoreline can not be ignored, the influence of bottom configuration on wave height transformation in a general three-dimensional bathymetry should also be examined.

Here a hydrodynamic model is presented considering the various effects of shoaling, wave breaking and energy absorption of soft mud bed on wave height transformation. Simulating the high energy dissipation of fluid mud layers, the proposed wave model can be applied on real field conditions.

Numerical Model

Rheological Model of Mud

Suitable rheological model of mud should be adopted in order to investigate

[DOR: 20.1001.1.17357608.1385.3.4.6.6]

wave-mud interaction. Mud in general can range from being a highly rigid and weakly viscous material to one that can be approximated as a purely viscous fluid, depending on the properties of the constituent sediment and the ambient fluid. Considering the complexity of rheological behavior, the visco-elastic-plastic model has been adopted in the present study to develop a predictive behavior model for wave-mud interaction [3]. The constitutive equations are expressed as:

$$\sigma_{ij} = 2\mu_e \dot{e}_{ij} \tag{1}$$

$$\mu_e = \begin{cases} \mu_1 + \dfrac{iG}{\omega} & (\frac{1}{2}\sigma_{ij}\sigma_{ij} \le \tau^2{}_y) \quad (2\text{-a}) \\ \mu_2 + \dfrac{\tau_y}{\sqrt{4|\Pi_e|}} & (\frac{1}{2}\sigma_{ij}\sigma_{ij} > \tau^2{}_y) \quad (2\text{-b}) \end{cases}$$

where σ_{ij} is the deviator part of stress tensor, $\dot{e}_{ij}$ is the deviator part of strain rate tensor, G is the shear modulus of elasticity, μ_1 is the viscosity of mud in the viscoelastic state, μ_2 is the viscosity of mud in the viscoplastic state, τ_y is yield stress, ω is the angular frequency of wave and $4|\Pi_e|$ is expressed as,

$$4|\Pi_e| = 2(\frac{\partial u}{\partial x})^2 + 2(\frac{\partial w}{\partial z})^2 + (\frac{\partial u}{\partial z} + \frac{\partial w}{\partial x})^2 \tag{3}$$

where u and w are velocity components in x and z direction, respectively. The rheological viscoelastic parameters of mud, i.e. shear modulus and viscosity, are calculated from the empirical equations offered by Shibayama and An [3]:

$$\mu_1 = 10^{(4.353 - 9.56\times10^{-3}W)} \times T \tag{4}$$

$$\log G = 4.761 - 1.05\times10^{-2}W + (0.147 - 3.38\times10^{-3}W) \times \log(T - 0.522 - 1.23\times10^{-3}W) \tag{5}$$

where T is the wave period and W is the water content of fluid mud (%). The viscoplastic parameters, μ_2 and τ_y are evaluated from the laboratory experiments of Tsuruya *et al.* [6].

Wave-Mud Interaction Model

Following Tsuruya et al. [6], the fluid system is divided into N layers in which the water layer is represented by N=1. Fig. 1 shows the sketch of the multi-layered model.

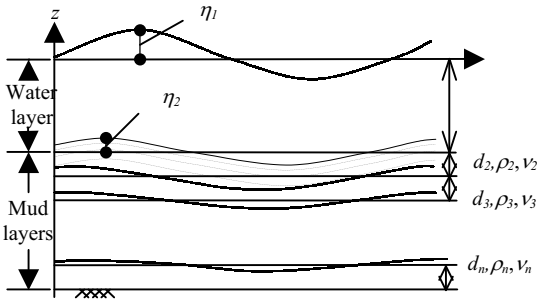

Fig. 1- Definition sketch of multi-layered model

The linearized Navier-Stokes equations, neglecting the convective accelerations, and the continuity equation for an incompressive fluid can be expressed as

$$\begin{cases} \dfrac{\partial u_j}{\partial t} = -\dfrac{1}{\rho_j}\dfrac{\partial p_j}{\partial x} + \nu_{e,j}(\dfrac{\partial^2 u_j}{\partial^2 x^2} + \dfrac{\partial^2 u_j}{\partial^2 z^2}) & (6\text{-a}) \\ \dfrac{\partial w_j}{\partial t} = -\dfrac{1}{\rho_j}\dfrac{\partial p_j}{\partial z} + \nu_{e,j}(\dfrac{\partial^2 w_j}{\partial^2 x^2} + \dfrac{\partial^2 w_j}{\partial^2 z^2}) & (6\text{-b}) \end{cases}$$

$$\frac{\partial u_j}{\partial x} + \frac{\partial w_j}{\partial z} = 0 \tag{7}$$

where x and z are the horizontal and vertical coordinates, the subscripts j indicate the layers, and the parameters t, ρ, ν_e and p represent the time, density, kinematic viscosity of mud and dynamic pressure, respectively.

The separable, periodic solutions for $\hat{u}_j$, $\hat{w}_j$ and $\hat{p}_j$ are assumed as

[DOR: 20.1001.1.17357608.1385.3.4.6.6]

$$\begin{cases} \hat{u}_j(x,z;t) = u_j(z)\exp[i(kx-\sigma t)] & \text{(8-a)} \\ \hat{w}_j(x,z;t) = w_j(z)\exp[i(kx-\sigma t)] & \text{(8-b)} \end{cases}$$

$$\hat{p}_j(x,z;t) = p_j(z)\exp[i(kx-\sigma t)] \quad \text{(8-b)}$$

where k is the unknown complex wave number, namely

$$k = k_r + i\,k_i \quad (9)$$

Displacements of water surface and interfaces, η_j, are represented as the following equation:

$$\eta_j = a_j \exp[i(kx-\sigma t)] \quad (10)$$

where a_j is the amplitude of the displacement of the j_{th} layer and the water surface is expressed as η_1.
Substituting the real and imaginary parts of wave number into Eq. (10), the expression of water surface and interfacial displacements can be obtained as

$$\eta_j = a_j \exp(-k_i x)\exp[i(k_r x-\sigma t)] \quad (11)$$

Therefore, the real part of the wave number, k_r, gives the wave length $L = 2\pi / k_r$ and its imaginary part, k_i, presents the wave attenuation rate, assuming the exponential wave height decay.
Substituting Eqs. (8-a) and (8-b) into the continuity Eq. (7) results to

$$u_j = \frac{iw_j'}{k} \quad (12)$$

where the prime represents the differential with respect to z. Introduction of Eq. (12) into Eq. (6-a) yields an expression for p_j

$$p_j = \frac{\rho_j \nu_{e,j}}{k^2}(w_j''' - w_j'\lambda_j^{\,2}) \quad (13)$$

where

$$\lambda_j^{\,2} = k^2 - i\sigma\nu_{e,j}^{\,-1} \quad (14)$$

Substituting p_j into the vertical momentum, Eq. (6-b), yields the forth order differential equation for w_j

$$w_j'''' - (k^2+\lambda_j^{\,2})w_j'' + k^2\lambda_j^{\,2}w_j = 0 \quad (15)$$

The solutions can be obtained as

$$w_j(z) = A_j \sinh k(\sum_{n=1}^{j} d_n + z) + B_j \cosh k(\sum_{ne1}^{j} d_n + z) + C_j \exp[\lambda_j(\sum_{n=1}^{j-1} d_n + z)] + D_j \exp[-\lambda_j(\sum_{ne1}^{j} d_n + z)] \quad (16)$$

where d_n is the thickness of n_{th} layer. The complex constants A_j, B_j, C_j, D_j, and the unknown variables k and a_j are determined from the boundary conditions.

• Boundary Conditions

5N boundary conditions are required for a viscous fluid model of N layers. The unknown constants and variables are determined from the boundary conditions at the water surface, the interfaces and the rigid bottom as follows

a. At the water surface ($z=\eta_1$)

The kinematic boundary condition, requiring the surface particles to follow the surface, and the imposition of zero normal and tangential stresses can be written as

$$\frac{\partial \eta_1}{\partial t} = \hat{w}_1 \quad (17)$$

$$\hat{p}_1 - 2\rho_1\nu_{e,1}\frac{\partial \hat{w}_1}{\partial z} = 0 \quad (18)$$

$$\rho_1\nu_{e,1}\left(\frac{\partial \hat{u}_1}{\partial z} + \frac{\partial \hat{w}_1}{\partial x}\right) = 0 \quad (19)$$

or after Taylor's expansion

$$A_1 \sinh kd_1 + B_1 \cosh kd_1 + C_1 + D_1 \exp(-\lambda_1 d_1) = -i\sigma a \quad (20)$$

$$M_1(A_1 \cosh kd_1 + B_1 \sinh kd_1) - 2\rho_1\nu_{e,1}\lambda_1[C_1 - D_1 \exp(-\lambda_1 d_1)] = \rho_1 g a_1 \quad (21)$$

[DOR: 20.1001.1.17357608.1385.3.4.6.6]

$$2A_1k^2\sinh kd_1 + 2B_1k^2\cosh kd_1 + (\lambda_1{}^2 + k^2)$$
$$[C_1 + D_1\exp(-\lambda_1 d_1)] = 0 \quad (22)$$

Where

$$M_1 = \frac{i\rho_1\sigma}{k} - 2\rho_1\nu_{e,1}k \quad (23)$$

$$\lambda_1{}^2 = k^2 - i\sigma\nu_{e,1}{}^{-1} \quad (24)$$

and g is the gravitational acceleration.

b. At the interfaces

The kinematic conditions which, due to the assumed linearity of the problem, are applied at $z_j = -\sum_{n=1}^{j} d_n$ can be written as

$$\frac{\partial\eta_{j+1}}{\partial t} = \hat{w}_j \quad (25)$$

or

$$B_j + D_j + C_j\exp(-\lambda_j d_j) = -i\sigma a_{j+1} \quad (26)$$

The continuity of horizontal and vertical velocities are

$$\hat{u}_j = \hat{u}_{j+1} \quad (27\text{-a})$$

$$\hat{w}_j = \hat{w}_{j+1} \quad (27\text{-b})$$

or

$$A_{j+1}\sinh kd_{j+1} + B_{j+1}\cosh kd_{j+1} + C_{j+1} + D_{j+1}$$
$$\exp(-\lambda_{j+1}d_{j+1}) = B_j + D_j + C_j\exp(-\lambda_j d_j) \quad (28)$$
$$kA_{j+1}\cosh kd_{j+1} + kB_{j+1}\sinh kd_{j+1} +$$
$$C_{j+1}\lambda_{j+1} - D_{j+1}\lambda_{j+1}\exp(-\lambda_{j+1}d_{j+1})$$
$$= kA_j + \lambda_j C_j\exp(-\lambda_j d_j) - \lambda_j D_j \quad (29)$$

The normal and tangential stresses are also continuous across the interfaces. Considering the Taylor series expansion about $z_j = -\sum_{n=1}^{j} d_n$, they can be written as

$$\hat{p}_j - 2\rho_j\nu_{e,j}\frac{\partial\hat{w}_j}{\partial z} - \rho_j g\eta_{j+1} = \hat{p}_{j+1} -$$
$$2\rho_{j+1}\nu_{e,j+1}\frac{\partial\hat{w}_{j+1}}{\partial z} - \rho_{j+1}g\eta_{j+1} \quad (30\text{-a})$$
$$\rho_j\nu_{e,j}\left(\frac{\partial\hat{u}_j}{\partial z} + \frac{\partial\hat{w}_j}{\partial x}\right)$$
$$= \rho_{j+1}\nu_{e,j+1}\left(\frac{\partial\hat{u}_{j+1}}{\partial z} + \frac{\partial\hat{w}_{j+1}}{\partial x}\right) \quad (30\text{-b})$$

or

$$M_jA_j - 2\rho_j\nu_{e,j}\lambda_j[C_j\exp(-\lambda_j d_j) - D_j]$$
$$= M_{j+1}(A_{j+1}\cosh kd_{j+1} + B_{j+1}\sinh kd_{j+1})$$
$$-2\rho_{j+1}\nu_{e,j+1}\lambda_{j+1}[C_{j+1} - D_{j+1}\exp(-\lambda_{j+1}d_{j+1})]$$
$$-(\rho_{j+1} - \rho_j)ga_{j+1} \quad (31\text{-a})$$
$$\rho_j\nu_{e,j}[2k^2B_j +$$
$$(\lambda_j{}^2 + k^2)(C_j\exp(-\lambda_j d_j) + D_j)] = \rho_{j+1}\nu_{e,j+1}$$
$$\{2k^2(A_{j+1}\sinh kd_{j+1} + B_{j+1}\cosh kd_{j+1})$$
$$+(\lambda_{j+1}{}^2 + k^2)[C_{j+1} + D_{j+1}\exp(-\lambda_{j+1}d_{j+1})]\} \quad (31\text{-b})$$

where

$$M_j = \frac{i\rho_j\sigma}{k} - 2\rho_j\nu_{e,j}k$$

c. At the rigid bottom

The velocities in both the horizontal and vertical directions should be zero at the fixed bottom, i.e.

$$\hat{u}_N = 0 \quad (32\text{-a})$$

$$\hat{w}_N = 0 \quad (32\text{-b})$$

or

$$kA_N - \lambda_N D_N + \lambda_N C_N\exp(-\lambda_N d_N) = 0 \quad (33\text{-a})$$

$$B_N + D_N + C_N\exp(-\lambda_N d_N) = 0 \quad (33\text{-b})$$

• Equivalent Viscosity

In the viscoplastic state of the visco-elastic-plastic model, the objective $4|\Pi_e|$ of the representative viscosity, see Eq. (2-b), can be approximated by a viscoelastic field using an iterative method. The real parts of Eqs. (8-a) and (8-b) may be written as

$$\hat{u}_j(z) = |u_j|\exp(-k_i x)\cos(k_r x - \sigma t + \alpha_j) \quad (34\text{-a})$$

$$\hat{w}_j(z) = |w_j|\exp(-k_i x)\cos(k_r x - \sigma t + \beta_j) \quad (34\text{-b})$$

where α_j and β_j are the arguments of u_j and w_j, respectively. Taking the partial derivatives of Eqs. (34-a) and (34-b) with respect to x and z

$$\frac{\partial \hat{u}_j}{\partial x} = -|k||u_j|\exp(-k_i x)\sin(k_r x - \sigma t + \alpha_j + \theta_k) \quad (35)$$

$$\frac{\partial \hat{u}_j}{\partial z} = -|u'_j|\exp(-k_i x)\cos(k_r x - \sigma t + \alpha'_j) \quad (36)$$

$$\frac{\partial \hat{w}_j}{\partial x} = -|k||w_j|\exp(-k_i x)\sin(k_r x - \sigma t + \beta_j + \theta_k) \quad (37)$$

$$\frac{\partial \hat{w}_j}{\partial z} = -|w'_j|\exp(-k_i x)\cos(k_r x - \sigma t + \beta'_j) \quad (38)$$

where α'_j and β'_j and θ_k are the arguments of u'_j, w'_j and k, respectively. Substituting Eqs. (35) ~ (38) into Eq. (3) leads to

$$4|\Pi_e| = \frac{1}{2}\{|k|^2(2|u_j|^2 + |w_j|^2) + (|u_j'|^2 + 2|w_j'|^2) - 2|u_j'||w_j||k|\sin(\beta_j + \theta_k - \alpha_j')\}\exp(-2k_i x) \quad (39)$$

• A result of wave-mud interaction model

Wave attenuation rate is taken as an example of calculated results of the wave-mud interaction model. Fig. 2 shows the changes of wave attenuation rate with respect to water depth for an 8.0 cm mud sample with water content of 128% [8]. The wave height and wave period of 44.0 cm and 6 s are adopted, respectively. As observed, wave attenuation rate decreases rapidly as the water depth increases. This reveals the necessity of using local values of wave attenuation rates at the computational grid points depending on the corresponding water depths.

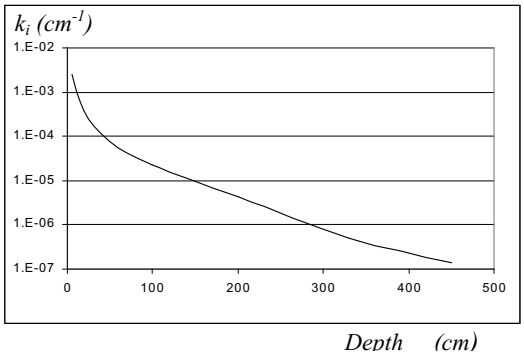

Fig. 2- Correlation between wave attenuation rate with water depth

ANN (Artificial Neural Network)

The calculations of wave attenuation rates in multi-layered model take considerable time as the number of nodes increases. Here ANN is proposed to speed up the calculation. It is a substitute for the multi-layered wave-mud interaction model when fully trained with the input and desired values calculated in the model.

A neural network is a machine that is designed to model the way in which the brain performs a particular task or function of interest; the network is usually implemented by using electronic components or is simulated in software on a digital computer. Particularly, a neural network is a massively parallel distributed processor made up of simple processing units called "neurons", which has a natural tendency for storing experiential knowledge and making it available for use. It resembles the brain in two respects; first, Knowledge is acquired by the network from its environment through a learning process. Second, interneuron connection strengths, known as synaptic weights, are used to store the acquired knowledge.

A popular paradigm of learning called learning with a teacher or supervised learning involves modification of the synaptic weights of a neural network by applying a set of labeled training samples or task examples. Each example consists of a unique input signal and a corresponding desired response. The network is presented with an example picked at random from the set, and the synaptic weights (free parameters) of the network are modified to minimize the difference between the desired response and the actual response of the network produced by the input signal in accordance with an appropriate statistical criterion [9].

[DOR: 20.1001.1.17357608.1385.3.4.6.6]

Recently, ANN has been used in a number of coastal engineering applications, due to their ability to approximate the nonlinear behavior without prior knowledge of the interrelations among the elements within a system. ANNs can be designed in various topologies, depending on how the neurons are structured and the learning algorithms, or rule used. In this study a feed-forward ANN with sigmoid and linear transfer functions in hidden and output layer are developed. This ANN is trained using the wave-mud interaction subroutine at the beginning of the wave transformation calculation for possible ranges of the wave heights, water depths and different mud thickness.The Topology of the ANN is shown in Fig. 3.

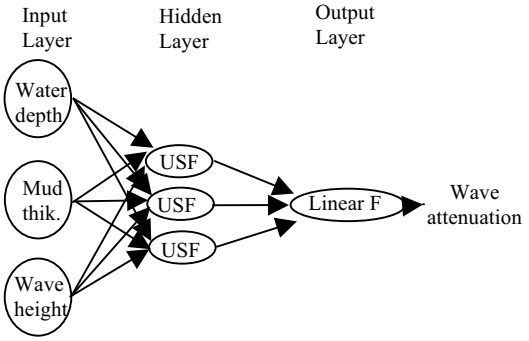

Fig. 3- ANN topology used in this study

The input layer consists of wave heights, water depths and mud thicknesses which cover the possible range of variations of a specific problem. The desired values are the wave attenuation rates that are calculated from the multi-layered wave-mud interaction model. A computer program is developed for back propagation learning scheme, in which not only the synoptic weights and biases, but also Unipolar Sigmoid transfer Functions (USF) parameters ($f(x)=\frac{2|a|}{1+e^{-2x|a|}}$ is USF where a is USF Parameter), are trained through gradient descendent algorithm. Training USF parameter improve convergence rate. In addition, the batch learning process is used for transfer functions parameters and normal training for biases and synoptic weights.
The learning process is summarized as below [10].

Fig. 4 shows the input of a sample neuron in a *(k+1)*-th layer of a network and its output and inputs from neurons in previous layer.

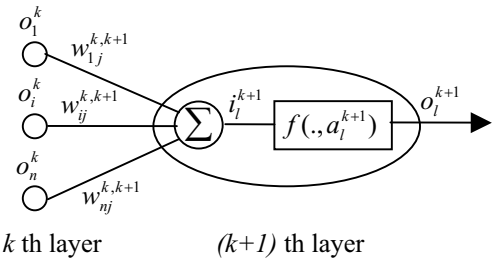

Fig. 4- Sample neuron in a network [10]

The cost function J_g is expressed as

$$J_g=\frac{1}{2}\sum_{i=1}^{L}(D_i-o_i^M)^2 \qquad (40)$$

where D and o_i^M represent desire values and output, respectively. Here M denotes output-layer and L is the number of units of output-layer. We shall try to change connection weights to minimize J_g, where $w_{ij}^{k-1,k}$ denotes a connection weight between the *i*-th *(k*-1*)-th* layer and the *j*-th *k*-th layer. Following the gradient descent algorithm, the increment $\Delta w_{ij}^{M-1,M}$ at the output-layer M can be expressed as

$$\Delta w_{ij}^{M-1,M}=-\eta\frac{\partial J_g}{\partial o_j^M}\frac{\partial o_j^M}{\partial i_j^M}\frac{\partial i_j^M}{\partial w_{ij}^{M-1,M}}$$

$$=-\eta\delta_j^M o_i^{M-1} \qquad (41)$$

$$i_j^M=\sum_i w_{ij}^{M-1,M}o_i^{M-1} \qquad (42)$$

here $\eta>0$ is learning rate given by small positive constant.

$$\delta_j^M = -\frac{\partial J_g}{\partial o_j^M}\frac{\partial o_j^M}{\partial i_j^M} = (t_j - o_j^M) f'(i_j^M) \quad (43)$$

where $f'(.)$ denotes $\partial f(i_j^M)/\partial i_j^M$, i_j^M is the input to the *j*-th neuron at the output layer M. The increment of the connection weights at hidden-layer, is similarly derived by

$$\Delta w_{ij}^{k-1,k} = -\eta \delta_j^k o_i^{k-1} \quad (44)$$

$$\delta_j^k = f'(i_j^k)\sum_i \delta_l^{k+1} w_{jl}^{k,k+1} \quad (45)$$

Thus, the resulting algorithms are described by

$$w_{ij}^{k-1,k}(t+1) = w_{ij}^{k-1,k}(t) + \eta \delta_j^k o_i^{k-1} + \alpha \Delta w_{ij}^{k-1,k}(t) \quad (46)$$

for the hidden-layer, and

$$w_{ij}^{M-1,M}(t+1) = w_{ij}^{M-1,M}(t) + \eta \delta_j^M o_i^{M-1} + \alpha \Delta w_{ij}^{M-1,M}(t) \quad (47)$$

for the output-layer, where t denotes the *t*-th update time and α is stabilizing (or momentum) coefficient defined in the range $0 \le \alpha < 1$.
From the same procedure for training USF Parameter we will get

$$a_i^M(t+1) = a_i^M(t) + \eta_2 \sigma_i^M f^*(i_i^M, a_i^M) + \alpha_2 \Delta a_i^M(t) \quad (48)$$

and

$$a_i^k(t+1) = a_i^k(t) + \eta_2 \sigma_i^k f^*(i_i^k, a_i^k) + \alpha_2 \Delta a_i^k(t) \quad (49)$$

Where

$$\Delta a_i^k = -\eta_2 \frac{\partial J_g}{\partial a_i^k} \quad (50)$$

$$\sigma_i^M = \frac{\partial J_g}{\partial o_i^M} \text{ and } \sigma_i^k = \frac{\partial J_g}{\partial o_i^k} \quad (51)$$

$$f^*(.,.) = \partial f(., a_i^k)/\partial a_i^k \quad (52)$$

$$f'(.,.) = \partial f(i_i^{k+1}, a_i^k)/\partial i_l^{k+1} \quad (53)$$

$$\sigma_i^k = \sum_l \sigma_l^{k+1} f'(i_l^{k+1}, a_l^{k+1}) w_{i,l}^{k,k+1} \quad (54)$$

Wave Transformation Model

The governing equations for wave transformation are time dependent mild slope equations which were introduced by Nishimura, Maruyama, and Hiraguchi [11]:

$$\frac{\partial Q_y}{\partial t} + c^2 \frac{\partial}{\partial y}(\xi) + f_D . Q_y = 0 \quad (55\text{-a})$$

$$\frac{\partial Q_x}{\partial t} + c^2 \frac{\partial}{\partial x}(\xi) + f_D . Q_x = 0 \quad (55\text{-b})$$

$$\frac{\partial \xi}{\partial t} + \frac{\partial (nQ_x)}{\partial x} + \frac{\partial (nQ_y)}{\partial y} = 0 \quad (55\text{-c})$$

where Q_x and Q_y are flow rates and ξ is water surface elevation. In these equations, c is wave celerity and $n=c_g/c$. f_D is the total dissipation coefficient which includes energy loss caused by wave-mud interaction (f_{DM}) before breaking line and both wave breaking and wave-mud interaction in the surf zone ($f_D = f_{DB} + f_{DM}$).

• Breaking Dissipation

Breaking dissipation coefficient is calculated as follows [12]:

$$f_{DB} = \alpha_D \tan\beta \sqrt{\frac{g}{h}\left(\frac{\hat{Q}}{Q_r} - 1\right)} \quad (56)$$

$$\hat{Q} = \sqrt{\hat{Q}_x^2 + \hat{Q}_y^2}, \quad Q_r = \gamma' \sqrt{gh^3}$$

where α_D and γ' are set to 2.5 and 0.25, respectively and $\tan\beta$ is the average bottom slope. The breaking point is determined using the breaker index, i.e. the ratio of the wave height to water depth (h_B / H_B), as a predefined value.

• Mud Dissipation

Theoretical and laboratory investigations indicated that the attenuation of wave height on a horizontal bed can be approximated by an exponential function [13-15]

[DOR: 20.1001.1.17357608.1385.3.4.6.6]

$$H(x) = H_0 e^{-k_i x} \tag{57}$$

where H_0 is the incident wave height at x=0, and k_i is the wave attenuation coefficient. The attenuation effect of mud is related to f_{DM} as below

$$\varepsilon_{Dm} = -\frac{d}{dx}(C_g E) = -C_g(2\rho g \frac{H}{8} \times \frac{dH}{dx}) = -C_g(\frac{2E}{H} \times \frac{dH}{dx})$$
$$= 2EC_g(-\frac{1}{H} \times \frac{dH}{dx}) = 2C_g k_i E \tag{58}$$

considering

$$\nabla.(c_g E) = -f_D n E \tag{59}$$

and

$$E = \rho g a^2 / 2 \tag{60}$$

it is concluded that in mild slope bottom bathymetry, $f_{DM} = 2k_i.c$.

• Discretization

The governing equations (55-a) to (55-c) are discretized following Horikawa [16]. It is assumed that the x-axis is directed from offshore towards shore, with the y-axis perpendicular to it, i.e. along the trend of the shoreline. The study area is divided into grid cells, each having a spacing of Δs in both the x- and y-directions, and the time increment is denoted by Δt. As shown in Fig. 4, a staggered mesh scheme is employed, in which the following notation is used:

$$Q^m_{xi,j} = Q_x\left\{i\Delta s, (j+\frac{1}{2})\Delta s, m\Delta t\right\} \tag{61-a}$$

$$Q^m_{yi,j} = Q_y\left\{(i+\frac{1}{2})\Delta s, j\Delta s, m\Delta t\right\} \tag{61-b}$$

$$\xi^m_{i,j} = \xi\left\{(i+\frac{1}{2})\Delta s, (j+\frac{1}{2})\Delta s, (m+\frac{1}{2})\Delta t\right\} \tag{61-c}$$

Eqs. (55-a) to (55-c) are discretized to yield

$$Q^{m+1}_{xi,j} = Q^m_{xi,j} - \frac{\Delta t}{\Delta s}(c_{xi,j})^2(\xi^m_{i,j} - \xi^m_{i-1,j}) - \Delta t(Q^m_{xi,j}) f_D \tag{62-a}$$

$$Q^{m+1}_{yi,j} = Q^m_{yi,j} - \frac{\Delta t}{\Delta s}(c_{xi,j})^2(\xi^m_{i,j} - \xi^m_{i,j-1}) - \Delta t(Q^m_{yi,j}) f_D \tag{62-b}$$

$$\xi^{m+1}_{i,j} = \xi^m_{i,j} - \frac{\Delta t}{\Delta s}\frac{1}{n_{i,j}}(n_{xi+1,j}Q^{m+1}_{xi+1,j} - n_{xi,j}Q^{m+1}_{xi.j} + n_{yi,j+1}Q^{m+1}_{yi,j+1} - n_{yi,j}Q^{m+1}_{yi,j}) \tag{62-c}$$

Eqs. (55-a) to (55-c), which include a nonlinear dissipation term with respect to the flow rate, should be solved for the computation of waves with the dissipation effects of mud and breaking. Since it cannot be discretized into an explicit form, the calculation over several cycles of the wave period is required to reach the final steady state solution for the whole area. Computation can be made by finite difference method using wave height values of the preceding wave calculation in dissipation term.

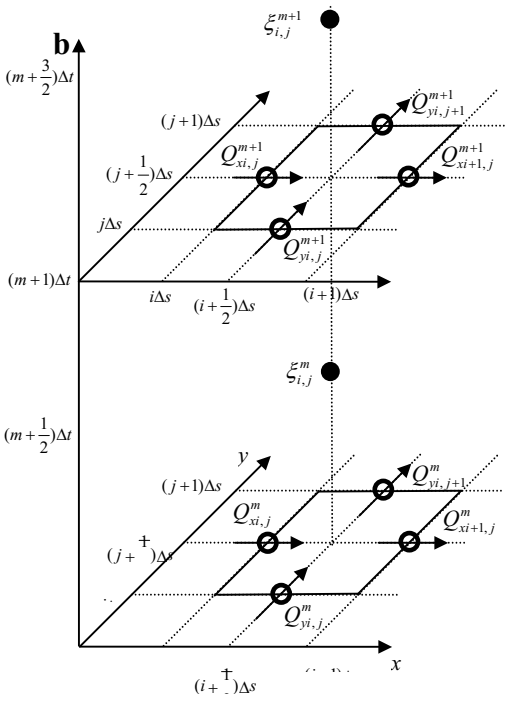

Fig. 4- Staggered mesh scheme

In order to include the breaking dissipation, $\hat{Q}$ in the equation of motion in the x-direction is computed by

$$\hat{Q}_{i,j} = [\{(\hat{Q}_{xi,j})^2 + \{(\hat{Q}_{yi,j} + \hat{Q}_{yi,j+1} + \hat{Q}_{yi-1,j+1} + \hat{Q}_{yi-1,j})/4\}^2]^{1/2} \tag{63-a}$$

and $\hat{Q}$ in the y-direction by

$$\hat{Q}_{i,j} = [\{\{\hat{Q}_{xi,j} + \hat{Q}_{xi+1,j} + \hat{Q}_{xi+1,j-1} + \hat{Q}_{xi,j-1})/4\}^2 + (\hat{Q}_{yi,j})^2]^{1/2} \quad (63\text{-b})$$

The grid spacing, Δs, should be small as compared to the wavelength in order to obtain an accurate solution. However, if the grid spacing is determined from the wavelength near the shoreline, it becomes too small to be practical for the whole study area. Therefore, the grid length is typically set to be 1/20 to 1/40 of the wavelength around a representative breaking point.

The time increment, Δt, must satisfy the following stability condition,

$$\Delta t \le \frac{\Delta s}{\sqrt{2} c_{\max}} \quad (64)$$

where $c_{\max}$ is the maximum value of the phase velocity in the study area.

• Boundary Conditions

a. Internal Boundaries with Arbitrary Reflectivity

Suppose partial standing waves exist in front of a reflective boundary along $x = x_0$, on which the reflection coefficient is k_R, and let α_n be the direction angle of the incident wave component, as shown in Fig. 5. The x-component of the flow rate at a certain time, t, at point (x_0, y_0) on the boundary and at another point $(x_0 - \Delta s, y_0)$ is given as the sum of the flow rates of the incident and reflected waves, Q_{xI} and Q_{xR}, by

$$Q_x^t(x_0, y_0) = Q_{xI}^t(x_0, y_0) + Q_{xR}^t(x_0, y_0) \quad (65)$$

$$Q_x^t(x_0 - \Delta s, y_0) = Q_{xI}^t(x_0 - \Delta s, y_0) + Q_{xR}^t(x_0 - \Delta s, y_0) \quad (66)$$

Expressing Q_{xI} and Q_{xR} as given by small-amplitude wave theory, and assuming a locally constant water depth, the following relation, valid for cases except $Q_x(x_0, y_0) = 0, k_R = 1$, is obtained:

$$Q_x^t(x_0, y_0) = A.Q_x^{t-\tau}(x_0 - \Delta s, y_0) \quad (67)$$

$$A = (1 - k_R)/\{1 + k_R^2 - 2k_R \cos(2k\Delta x s \cos\alpha_n)\}^{1/2} \quad (68)$$

$$\tan\sigma\tau = \frac{1 + k_R}{1 - k_R} \tan(k\Delta s \cos\alpha_n) \quad (69)$$

This relation means that the flow rate at point (x_0, y_0) on the boundary at time t is given by multiplying the flow rate at the inner point $(x_0 - \Delta s, y_0)$ at time $t - \tau$ by coefficient A.

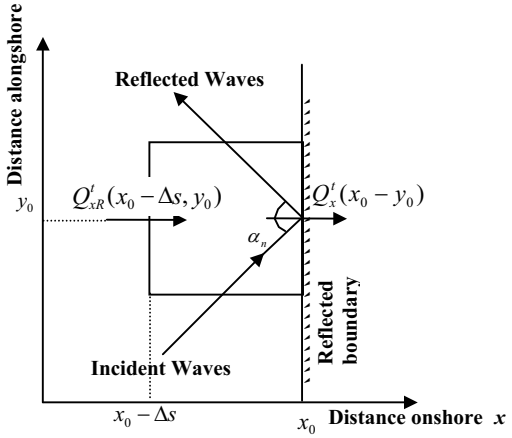

Fig. 5- Boundary with arbitrary reflectivity

For a boundary parallel to the x-axis, the y-component of the flow rate is similarly given by

$$Q_y^t(x_0, y_0) = A.Q_y^{t-\tau}(x_0, y_0 - \Delta s) \quad (70)$$

b. Nonreflective Virtual Boundaries

Side boundaries of the computation area are generally virtual open boundaries established for performing the numerical analysis. The presence of such virtual boundaries should not affect

[DOR: 20.1001.1.17357608.1385.3.4.6.6]

the solution in the study area. For this, the side or lateral boundaries are treated as having no reflection $(k_R = 0)$, so that waves pass freely through them. Namely, if an open boundary is parallel to the *x*-axis, then

$$Q_x^t(x_0, y_0) = Q_x^{t-\tau}(x_0 - \Delta s, y_0) \quad (71)$$

$$\tau = \Delta s.\cos\alpha_n / c \quad (72)$$

whereas for a boundary parallel to the *y*-axis,

$$Q_y^t(x_0, y_0) = Q_y^{t-\tau}(x_0, y_0 - \Delta s) \quad (73)$$

c. Offshore Open Boundary

Incident wave conditions are typically given on the offshore boundary to initiate the calculation. It is incorrect to specify the flow rates there as equal to those of only the incident waves, because in general there exist not only incident waves but also outgoing wave components across the offshore boundary due to the reflection from structures and the shoreline. Such outgoing waves should be freely transmitted through the boundary.

The situation of incident waves with an amplitude, a_I, and a directional angle, α_I, together with outgoing waves as shown in Fig. 6 is considered. Applying a procedure similar to that adopted for a nonreflective virtual boundary, the flow rates on an offshore open boundary is set as

$$Q_x^t(x_0, y_0) = a_1 c \cos\alpha_1 \sin(kx_0 \cos\alpha_1 + ky_0 \sin\alpha_1 - \sigma t) + Q_{xR}^{t-\tau}(x_0 + \Delta s, y_0)$$

$$\tau = \Delta s.\cos\alpha_n / c$$

where

$$Q_{xR}^t(x_0 + \Delta s, y_0) = Q_x^t(x_0 + \Delta s, y_0) - a_1 c \cos\alpha_1 \sin\{k(x_0 + \Delta s)\cos\alpha_1 + ky_0 \sin\alpha_1 - \sigma t\}$$

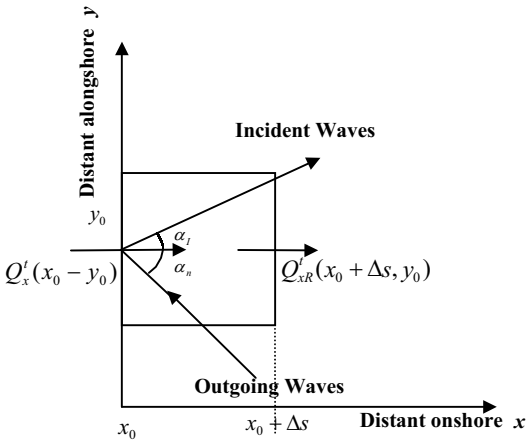

Fig. 6- Offshore open boundary

Procedure of Calculation

Fig. 7 shows the flow chart of the simulation procedure. The input data consists of the necessary information including offshore wave height and wave period, bottom topography and fluid mud characteristics.

At first, wave-mud interaction model is utilized for calculating wave attenuation rate k_i for the ranges of the wave heights, fluid mud thicknesses and water depths that may be applied. These values are then used for training ANN. Considering that k_i should be calculated at each grid point, the repetitive computations of wave-mud interaction model takes a considerable portion of the total consuming time if the number of grid points increase. This highly time-consuming calculation of wave attenuation rate is considerably decreased by using ANN.

[DOR: 20.1001.1.17357608.1385.3.4.6.6]

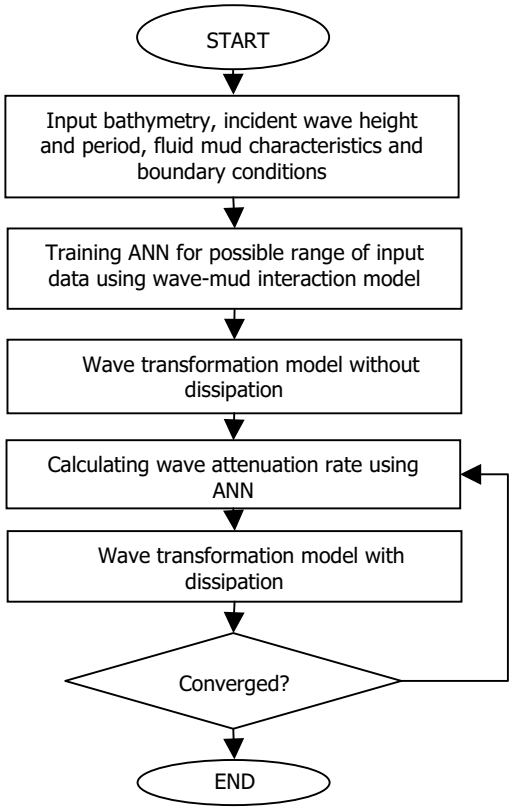

Fig. 7- Flow chart of the simulation procedure

Wave model is used to compute wave height transformation at the next step. Wave attenuation rate on each grid location is predicted by ANN regarding the wave height, fluid mud thickness and water depth at the specific node. The corresponding wave energy dissipation rate is used to calculate the wave height at the next grid point. Inside the surf zone, the energy dissipation of fluid mud layer is combined with the one due to wave breaking.

Model performance

In this section, the applicability of the hydrodynamic model will be examined. Two examples of numerical computations are presented. The first one is a comparison of the developed wave model, based on the time-dependent mild slope equations, with the Parabolic Mild Slop (PMS) Module of MIKE 21. The aim of this comparison is to check the overall behavior of the numerical model, assuring the correctness of calculations. No energy dissipation of bottom layer is included in the numerical simulations assuming that the wave is propagating on a fixed bed.

The second example shows a comparison of wave height distribution on a general bathymetry where the fluid mud layer exists.

Comparison with PMS module of MIKE 21

The model is applied for the East Bay, Louisiana with the assumption of fixed bed in order to compare the model result with the result of PMS module of MIKE 21. The bathymetry is shown in Fig. 8.

Fig. 9 shows the comparison of wave height results. All the boundaries of the model, except left boundary which is an offshore open boundary, are nonreflective Virtual Boundaries. Incident wave is a regular one with 0.57 (m) in height perpendicular to left border. A reasonable agreement can be observed between the two simulations. The slight difference is probably due to the differences in formulation and imposing boundary conditions.

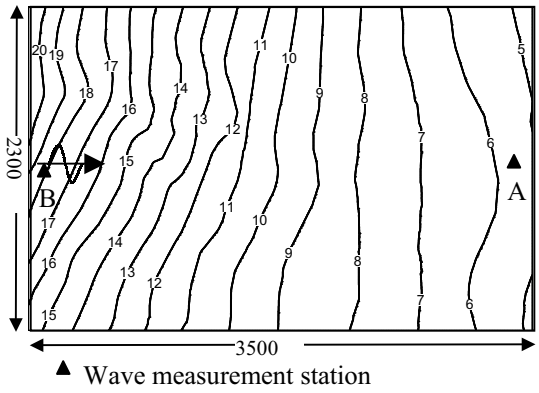

Fig. 8- Bathymetry and the wave measurement stations

[DOR: 20.1001.1.17357608.1385.3.4.6.6]

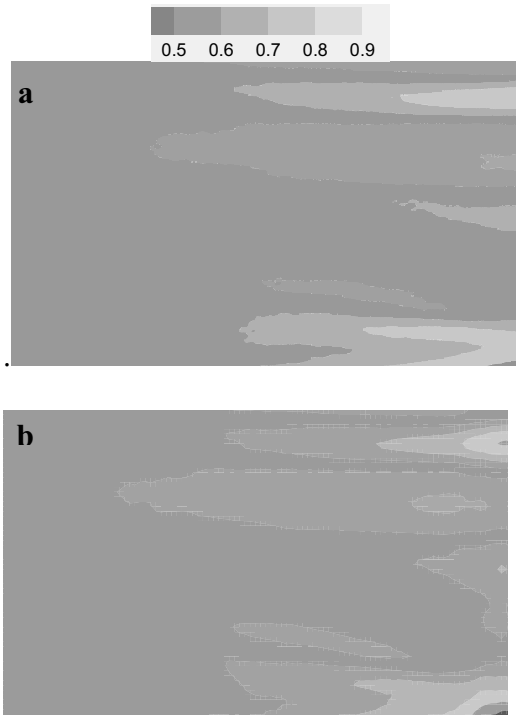

Fig. 9- Comparison of the wave height transformations on a fixed bed a) MIKE 21, b) Present model

Comparison with field data

The model is applied for the East Bay, Louisiana with recently deposited material from Mississippi River [13]. This deposition is very soft with shear strength ranges from 1.57 KPa near the water/sediment interface to 2.36 KPa three meters into the sediment. The bottom contours are shown in Fig. 8. The wave period was 7.75 s and the measured wave heights were 0.54 m at B and 0.285 m at A. The wave height at B is set to be 0.54 m and the wave height transformations are calculated. The resulted wave heights are depicted in Fig. 10.

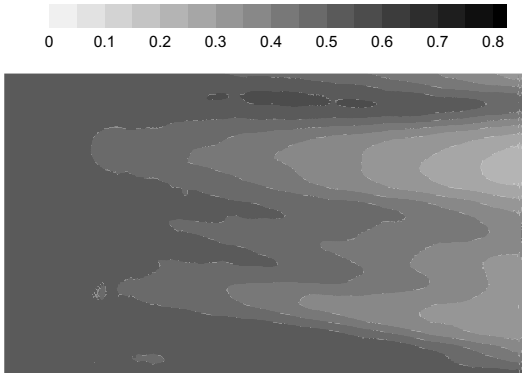

Fig. 10- Wave height contours on 70 cm thick fluid mud layer

Table 1 shows the calculated results at station A assuming different values of thicknesses of fluid mud layer. The measured data at station A, i.e. 28.5 cm, is in agreement with the fluid mud depth of about 70-100 cm. Although the actual distribution of fluid mud in the area is not known, this average thickness is well between the usual depths of fluid mud in Louisiana coast, i.e. 20-150 cm, as reported by Wells [14].

Table 1- Mud layer thickness and relative wave height

Fluid mud layer thickness (cm)	100	70	50
Wave height at station A (cm)	17	35	62

Conclusion

The wave attenuation on fluid mud was successfully simulated as a part of dissipation term in mild slope equations considering multi-layer visco-elastic-plastic model. The two dimensional numerical model includes combined wave refraction, diffraction, reflection, breaking and wave attenuation due to wave-mud interaction. Model performance was tested with available measurement data showing a reasonable agreement with field measurements. However, more data is necessary to evaluate the accuracy of the numerical simulation.

References

1- Sakakiyama, T. and Bijker, E. W. (1989): "Mass transport velocity in mud due to progressive waves" , Report of Coastal Engineering Group, Coastal Engineering Division, Delft University of Technology.

2- Ross, M. A. and Mehta, A. J. (1990): "Fluidization of soft estuarine mud by waves ", In The Microstructure of Fine Grained Sediments: From Mud to Shale, R. H. Bennett ed., Springer-Verlag, New York, pp. 185-191.

3- Shibayama, T. and An, N. N. (1993): "A visco-elastic-plastic model for wave-mud interaction", Coastal Engineering in Japan, Vol. 36, No. 1, pp. 67-89.

4- Shibayama, T., Aoki, T., and Sato, S. (1989): "Mud mass transport rate due to waves": a viscoelastic model, 1989, IAHR, pp. B567-B574.

5- Soltanpour, M., Shibayama, T. and Noma, T. (2003): "Cross-shore mud transport and beach deformation model", Coastal Engineering Journal, Vol. 45, No. 3, pp. 363-386.

6- Tsuruya, H., Nakano, S. and Takahama, J. (1987): "Interaction between surface waves and a multi-layered mud bed", Rep Port and Harbor Res. Inst., Ministry of Transport, Japan, Vol. 26, No. 5, pp. 141-142.

7- Soltanpour, M. (1999): "Two-dimensional modeling of mud profile processes", PhD Dissertation, Yokohama National University, 165 p.

8- Shibaiama, and T. Soltanpour, M. (1998): "Two dimensional of mud beach transformation in surfzone by using visco-elasto-plastic model of mud" Proc. of Coastal Engineering, JSCE, Vol. 45, pp. 521-525 (in Japanese).

9- Haykin, S. (1999): "Neural network: A Compressive Foundation" Prentice Hall, NJ.

10- Teshnelab M. and Watanabe, K. (1999): "Intelligent Control Based on Flexible Neural Networks" Kluwer Academic Publication.

11- Nishimura, H., K. Maruyama, and K. Hiraguchi, (1983): "Wave field analysis by finite difference method", Proc. 30nd Japanese Conf. on Coastal Eng., JSCE, pp. 123-127 (in Japanese).

12- Watanabe, A., and Maruyama, K. (1986): "Numerical modeling of nearshore wave field under combined refraction, diffraction and breaking," Coastal Engineering in Japan, Vol. 29, pp. 19-39.

13- Keulegan, G. H. (1950): "Wave motion." Engineering Hydraulics, John Wiley and Sons, New York, Chapter 11.

14- Gade, H. G. (1958): "Effects of a non-rigid, impermeable bottom on plane surface waves in shallow water." Journal Marine Research, 16(2), pp. 61-82.

15- Iwasaki, T., and Sato, M. (1972). "Dissipation of wave energy due to opposing current" Proc. 13th Coastal Eng. Conf. ASCE, pp. 605-622.

16- Horikawa K. (1988): "Nearshore dynamics and coastal processes," University of Tokyo Press.

17- Tubman, M.W., and J. N., Suhayda (1976): "Wave action and bottom movements in fine sediments", Proc. 15-th Coastal Eng. Conf., pp. 1168-1183.

18- Wells, J. T. (1983): "Dynamics of coastal fluid muds in low-, moderate-, and high-tide-range environments", Can. Journal Fisheries and Aquatic Sci., 40(1), pp.130-142.

[DOR: 20.1001.1.17357608.1385.3.4.6.6]